JACS
JOURNAL OF THE AMERICAN CHEMICAL SOCIETY
Article
pubs.acs.org/JACS

High-Spin S = 2 Ground State Aminyl Tetraradicals

Andrzej Rajca,*[,†] Arnon Olankitwanit,[†] Ying Wang,[†] Przemysław J. Boratyński,[†,§] Maren Pink,[‡] and Suchada Rajca[†]

[†]Department of Chemistry, University of Nebraska, Lincoln, Nebraska 68588-0304, United States
[‡]IUMSC, Department of Chemistry, Indiana University, Bloomington, Indiana 47405-7102, United States

Supporting Information

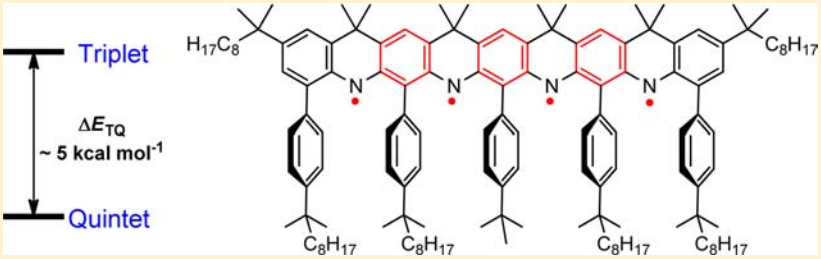

ABSTRACT: Aminyl tetraradicals with planar tetraazanonacene backbones have quintet (S = 2) ground states and do not show any detectable thermal population of the low-spin excited states up to the highest temperature investigated (100 K) in the 2-methyltetrahydrofuran (2-MeTHF) matrix. This indicates that the nearest electronic excited state (triplet) is at least ~0.3 kcal mol^{-1} higher in energy, that is, the triplet−quintet energy gap, ΔE_{TQ} > 0.3 kcal mol^{-1}, which is consistent with the broken-symmetry-DFT-computed ΔE_{TQ} of about 5 kcal mol^{-1}. In concentrated (ca. 1−10 mM) solutions of tetraradical **4** in 2-MeTHF at 133 K, a fraction of tetraradicals form a dimer (association constant, $K_{assoc} \approx 60$ M^{-1}), with a weak, antiferromagnetic exchange coupling, $J/k \approx -0.1$ K ~ 0.2 cal mol^{-1}, between the S = 2 tetraradicals. This weak intradimer exchange coupling is expected for two tetraradicals at the distance of about 6 Å. The most sterically shielded tetraradical **5** in 2-MeTHF has a half-life of 1 h at room temperature; the product of its decay is the corresponding tetraamine, suggesting that the hydrogen atom abstraction from the solvent is primarily responsible for the decomposition of the tetraradical.

INTRODUCTION

π-Conjugated organic diradicals and polyradicals that possess high-spin ground states (total spin quantum number $S \geq 1$) are of fundamental interest in chemistry and physics.[1−3] The spin alignment in high-spin molecules is antithesis to spin pairing in chemical bonds,[1a,4,5] and it provides enhanced paramagnetism that is scaling with the $S(S + 1)$ factor. Molecules with strong paramagnetic properties are important in the development of spintronics,[6] paramagnetic relaxation reagents,[7] including contrast agents in magnetic resonance imaging.[8,9] Furthermore, high-spin molecules are building blocks for organic magnetic materials.[10,11] To take advantage of the enhanced paramagnetic properties, the diradical or polyradical should be persistent at room temperature and its high-spin ground state must be exclusively populated. The energy gap (ΔE) between the high-spin state and the lowest low-spin excited state should be significantly greater than the thermal energy (RT) at 298 K. Such diradicals and polyradicals are exceptional and, especially those with very large values of S, are challenging to attain.[12−16]

Recently, we reported aminyl diradicals **1**−**3** that possess triplet ground states (Figure 1).[15−17] These diradicals are rare examples of persistent aminyl radicals ($R_2N\cdot$), which are typically detected as reactive intermediates.[18,19] Notably, diradical **2** possesses adequate persistence at room temperature for isolation as a solid diradical that could be stored under inert atmosphere at −20 °C for months incurring only slight decomposition. Diradicals **1**−**3** are predicted by calculations to possess large singlet−triplet energy gaps, ΔE_{ST} of 5−10 kcal mol^{-1} (Figure 1). In these structures, coplanarity of the two aminyl radicals and *m*-phenylene moiety facilitates the delocalization of spin density into the *m*-phenylene moiety, and thus large values of ΔE_{ST}.[1a,15−17,20] State of the art dedicated difference configuration interaction (DDCI) calculations by Barone and co-workers predict values of ΔE_{ST} = 5.5 and 9.6 kcal mol^{-1} for **1** and **3**, respectively,[21] which are in qualitative agreement with ΔE_{ST} values determined by broken-symmetry density functional theory (BS-DFT) calculations, as well as with the limiting values of ΔE_{ST} determined by superconducting quantum interference device (SQUID) magnetometry for **1**−**3** (Figure 1).[15−17] The DDCI calculations also predict that ΔE_{ST} for the nitroxide ($R_2NO\cdot$) diradicals structurally related to **1**−**3** are decreased by 1 order of magnitude,[21,22] in agreement with $\Delta E_{ST} \geq 0.6$ kcal mol^{-1} measured by SQUID magnetometry for the planar diazapentacene-based nitroxide diradical related to **1** and **2**.[23,24] In general, the decreased ΔE_{ST} may be associated with diminished delocalization of spin density in nitroxide radicals and other organic radicals stabilized by resonance.[1a,25]

Received: September 17, 2013
Published: November 4, 2013

 © 2013 American Chemical Society dx.doi.org/10.1021/ja409472f | J. Am. Chem. Soc. 2013, 135, 18205−18215

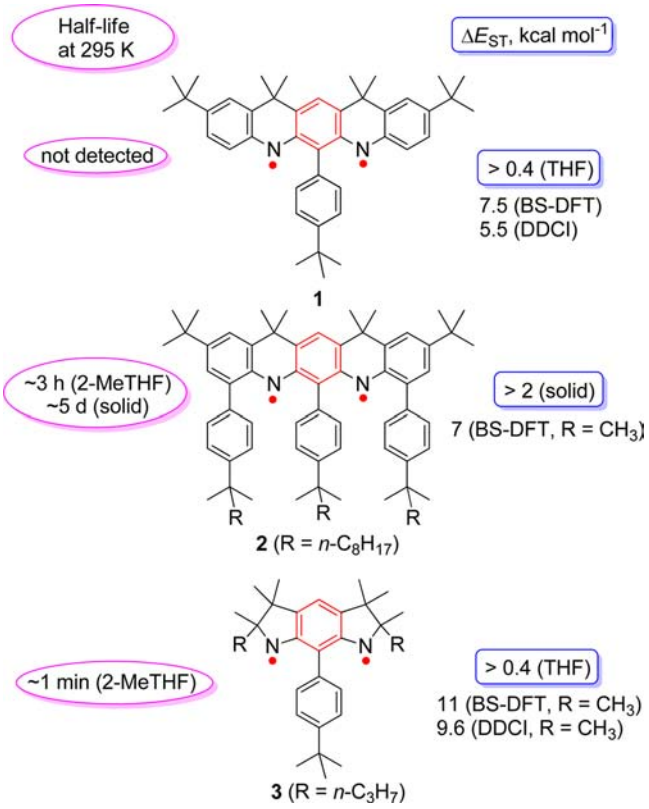

Figure 1. Persistent, triplet ground state aminyl diradicals: half-life at room temperature and singlet−triplet energy gap, determined experimentally by SQUID magnetometry and computationally by BS-DFT and DDCI.

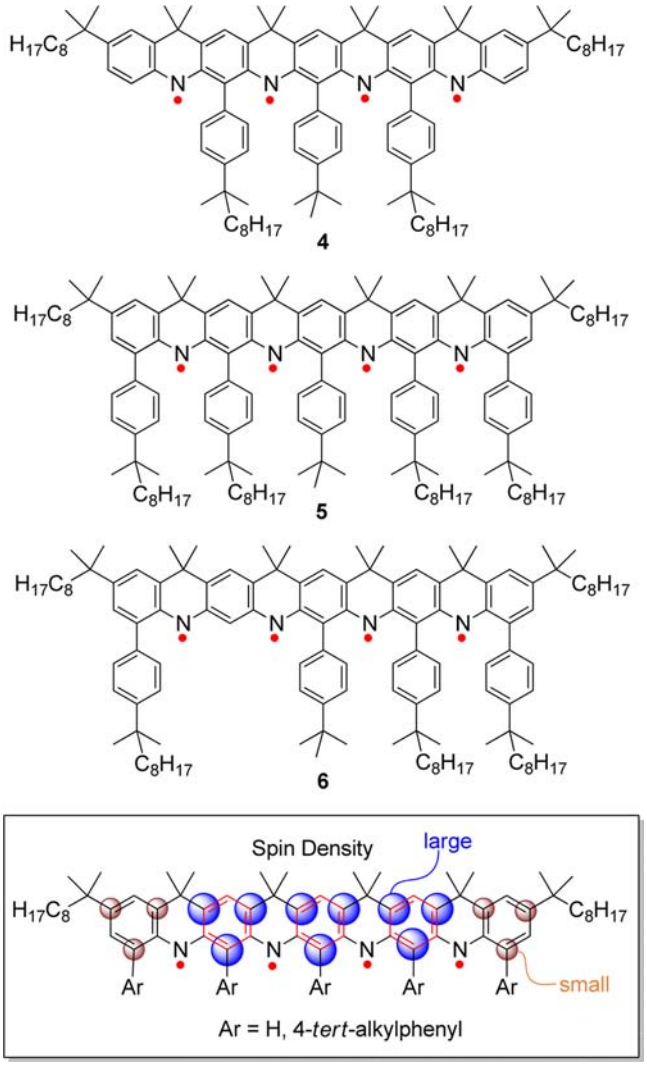

Figure 2. High spin aminyl tetraradicals **4**−**6** with planar tetraazanonacene backbones.

Herein we report the synthesis and magnetic characterization of aminyl tetraradicals **4**−**6** (Figure 2). In **4**−**6**, planarity of the tetraazanonacene backbone assures an effective $2p_\pi$−$2p_\pi$ overlap within the cross-conjugated π-system of aminyl radicals and *m*-phenylenes, leading to an $S = 2$ (quintet) ground state separated from low spin excited states by energy gaps ΔE on the order of 5 kcal mol^{-1}. The carbon and nitrogen atoms with significant spin densities are sterically shielded to enhance persistence of tetraradicals but without perturbing the planarity of their tetraazanonacene backbones (Figure 2). The most sterically shielded tetraradical **5**, possessing five 4-*tert*-alkylphenyl pendants, has a half-life of 1 h in 2-methyltetrahydrofuran at room temperature.

RESULTS AND DISCUSSION

Synthesis of Ladder Tetraamines. Tetraamine **7** (Scheme 1) with the ladder structure of nine collinearly fused rings was previously prepared via a convergent route by palladium-catalyzed C−N coupling reactions and Friedel−Crafts-like annelations forming six-membered rings.[26,27] However, the analogous convergent route to tripendant tetraamine **10** was not successful, presumably due to increased steric hindrance of the *ortho*-substitution in the C−N coupling reaction.[28] We developed a divergent route to **10** and **11**, starting with the di- and tetra-bromination step, followed by Suzuki coupling (Scheme 1). However, the bromination of **7** under a range of conditions, including those employed for the tribromination step in the synthesis of tripendant diamine **13** (Chart 1),[15,17] results in complex, dark-colored mixtures with broad ^{1}H NMR spectra. Bromine (Br_2, $E^{+/0} \approx 0.5$ V vs SCE)[29] can oxidize tetraamine **7** ($E^{+/0} \approx 0.5$ V and $E^{2+/+} \approx 0.6$ V vs SCE),[25] to the corresponding aminium radical cation and diradical dication, and therefore we trapped the electrophilic radical cation intermediate with an excess of bromide under strictly anhydrous conditions at low temperature. This method provides dibromotetraamine **8** and tetrabromotetraamine **9** in good yields. Suzuki coupling of the brominated tetraamines with pinacol 4-*tert*-undecylphenylboronate[15] provides the target tetraamines **10** and **11**, as well as tetra-pendant tetraamine **12**, in moderate yields.

Structure of Ladder Tetraamines. The X-ray structure of tetraamine **11** shows that the nine collinearly fused six-membered rings form a nonplanar, buckled π-system, with boat-like conformations for the NH-containing six-membered rings (Figure 3). Absolute values of torsional angles such as C2−C3−C4−C5 and C31−N1−C32−C33 in **11** are approximately 150° (Table S2, Supporting Information). A similar conformation was observed in the X-ray structure of tetraamine **7**.[26]

Notably, the structure of tetraamine **11** with buckled π-system is distinct from the previously reported X-ray structures of diamine **13** and tetraamine **14** (Chart 1) which showed planar π-systems of the five and nine collinearly fused six-membered rings, respectively.[15,26]

dx.doi.org/10.1021/ja409472f | J. Am. Chem. Soc. 2013, 135, 18205−18215

Scheme 1. Synthesis of Ladder Tetraamines 10−12

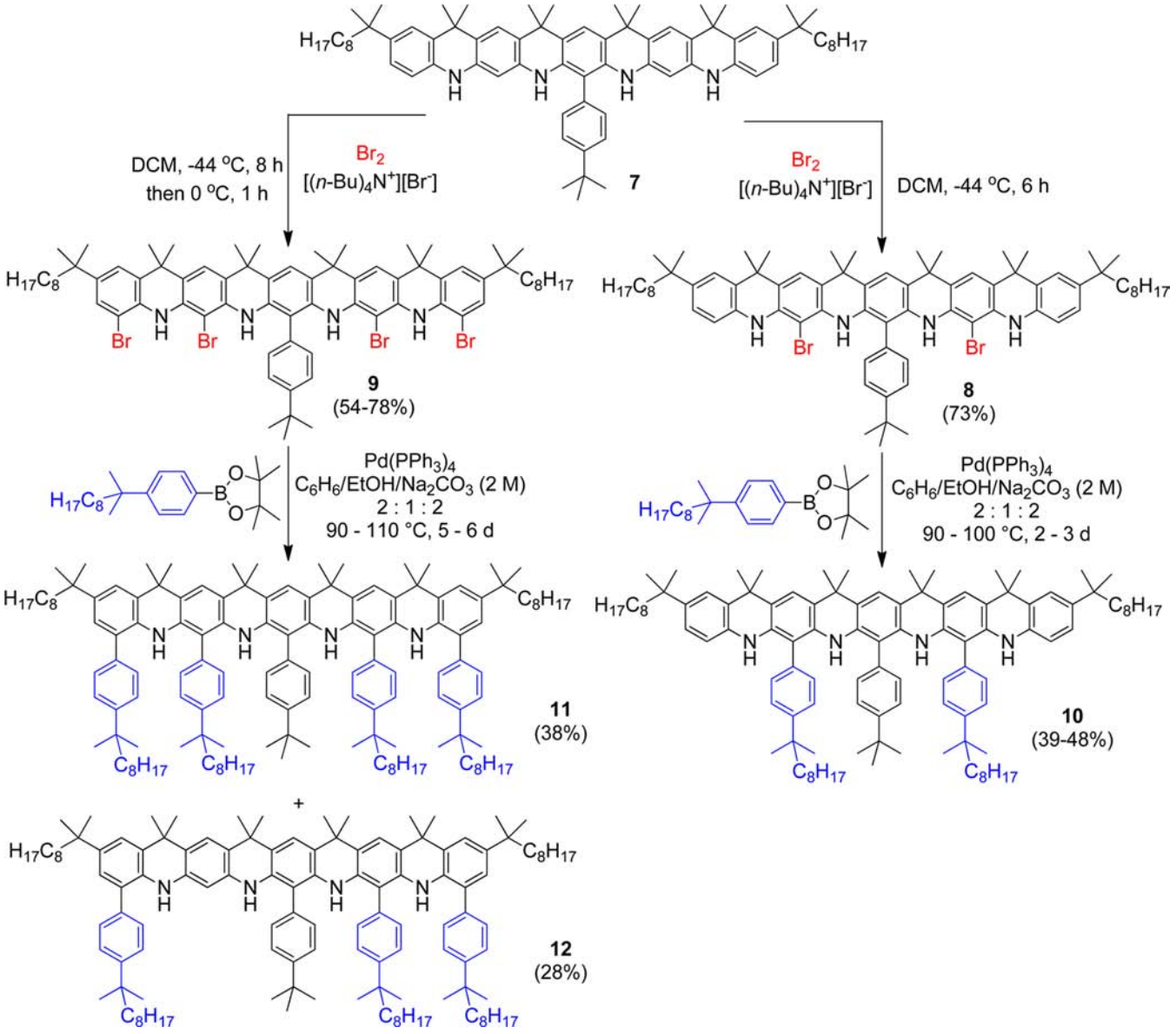

Chart 1. Diamine 13 and Tetraamine 14

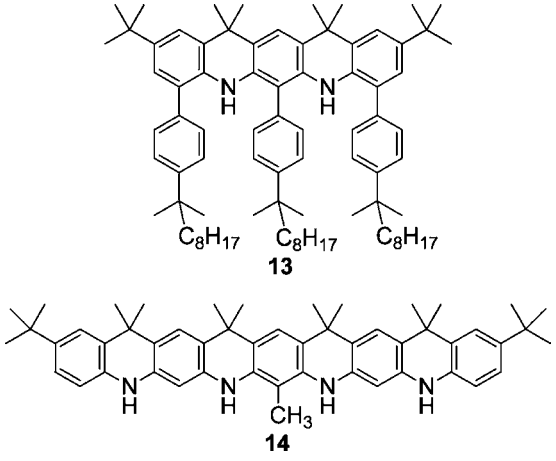

To gain better insight into the structures of these sterically hindered tetraamines with π-systems of collinearly fused six-membered rings, we carried out computational modeling. The simplified structures of **10**−**13**, in which the *tert*-undecyl groups are replaced with *tert*-butyl groups (**10a**−**13a**), are studied at the B3LYP/6-31G(d,p) level of theory.[32] Full geometry optimizations of these structures with planar (**10a**−**13a**) or buckled (**10a**, **11a**, and **13a**) conformations provide similar minimum energies—within about 1 kcal mol^{-1}. In the buckled conformation of **11a**, the geometry of the tetraazanonacene moiety, as described by the selected angles and torsional angles, is similar to that in the X-ray structure of **11** (Table S2, Supporting Information). The vibrational analyses for both the planar- and buckled-tetraamine with three pendants, **10a**, and diamine with three pendants, **13a**, suggest that their fused ring moieties are flexible with low frequencies of 5−10 cm^{-1} for the symmetric out-of-plane vibrational modes (Table S6, Supporting Information). This suggests that the duality of conformations determined by the X-ray structures for the collinearly fused ring moieties may be a result of packing effects.

Structures of tetraamines **10**−**12** are confirmed by the assignment of their experimental ^{1}H and ^{13}C NMR spectra in

dx.doi.org/10.1021/ja409472f | J. Am. Chem. Soc. 2013, 135, 18205−18215

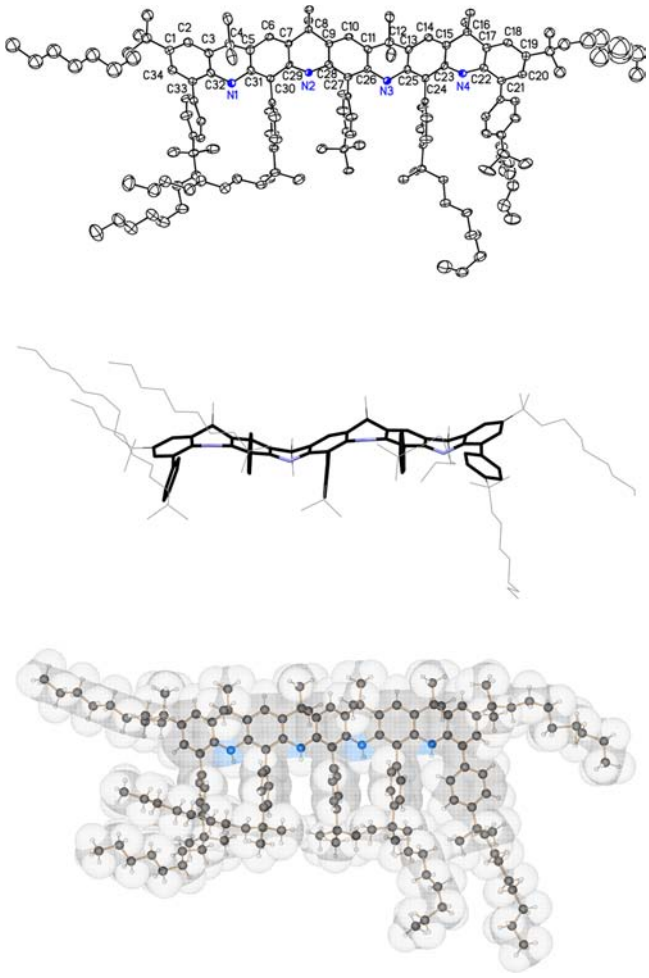

Figure 3. Molecular structure and conformation for **11**: Ortep plot (top), Mercury-generated[30] side view showing buckling of the fused ring moiety (middle) and Schakal-generated[31] space-filling plot (bottom). In the Ortep plot, carbon and nitrogen atoms are depicted with thermal ellipsoids at 50% probability; disorder and hydrogens are omitted for clarity. Further details are reported in Tables S1 and S2, and Figures S1 and S2 in the Supporting Information.

benzene-d_6 using standard 2D NMR spectroscopy, including ^{1}H−^{13}C HSQC, ^{1}H−^{13}C HMBC, ^{1}H−^{1}H NOESY, and ^{1}H−^{15}N HSQC (Figures S5−S9 and S18−S47, Supporting Information). Diamine **13**, for which the X-ray structure was determined,[15] was subjected to similar NMR experiments in chloroform-*d* and serves as a reference for the tetraamines.

Additional structural evidence for the pendant-substituted ladder tetraamines was obtained from the correlation between the DFT-calculated (δ_{DFT}) and experimental (δ_{expt}) ^{1}H and ^{13}C NMR chemical shifts. Using the calculated chemical shifts for **10a**−**13a** with planar fused ring moieties (Figures S10 and S11, Supporting Information), correlation coefficients, R^2 = 0.996−0.997 and 0.991−0.997, are obtained for ^{1}H and ^{13}C NMR chemical shifts, respectively (Table S11, Supporting Information). Also, the calculated ^{1}H and ^{13}C NMR chemical shifts for tetraamine **11a**, with buckled π-system of collinearly fused six-membered rings similar to the conformation found in the X-ray structure of **11**, provide correlations similar to those of planar **11a** (Figures S16 and S17, Supporting Information). The relationship between computed and experimental NMR chemical shifts is further illustrated by applying the correlations to scale linearly δ_{DFT} that provide δ_{scaled}, and then by plots of the differences between the scaled and experimental NMR chemical shifts ($\delta_{scaled} - \delta_{expt}$) for each distinct carbon or hydrogen atom in the structure (Figures S11−S15, Supporting Information). These plots confirm good agreement between theory and experiment, specifically the low values of statistical error parameters for ^{13}C and ^{1}H (with the NH groups excluded) NMR chemical shifts (Table S11, Supporting Information).[26,33−36]

Aminyl Tetraradicals. We first attempted to prepare aminyl tetraradicals **15** and **16** from the recently reported ladder tetraamines **7** and **14** (Scheme 2)[26] under the reaction

Scheme 2

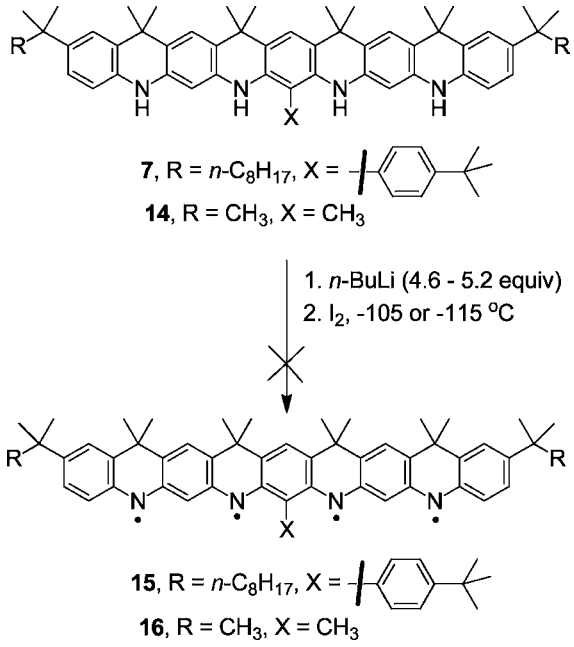

conditions for generation of aminyl diradicals at low temperatures; that is, a slight excess of *n*-BuLi over the stoichiometric amount of 4 equiv is added to the tetraamine, and then the reaction mixture is oxidized. Iodine is added by vacuum transfer in small portions (Scheme 2).[15−17] In each case, the EPR spectra of the reaction mixture show an intense center peak, side bands, and a half-field ($|\Delta m_s| = 2$) transition. The side bands could be simulated with the EPR spectral parameters similar to those for the S = 1 state of aminyl diradicals **1** and **2**.[15,17] The crude reaction mixture obtained from oxidation of tetraamine **14** was investigated by SQUID magnetometry and only an "average" value of $S \approx 1$ was obtained. MALDI MS studies on the crude reaction mixture derived from tetraamine **7** showed dominant peaks at an m/z corresponding to oligomers of **15** (or **7**), and relatively insignificant peak intensity at an m/z of **7** (Figures S48−S54, Supporting Information).

These results indicate that only a fraction of the expected radicals (unpaired electrons) could be detected in the reaction mixtures and may imply that the targeted tetraradicals are not persistent even at low temperatures, and most likely form covalently bonded oligomers.

Aminyl tetraradicals **4**−**6** are prepared from tetraamines **10**−**12**. Deprotonation of tetraamine (∼1 mg, ∼0.5 μmol) with *n*-BuLi provides solutions of the corresponding tetraanion in tetrahydrofuran/hexanes. After solvent exchange to 2-methylte-

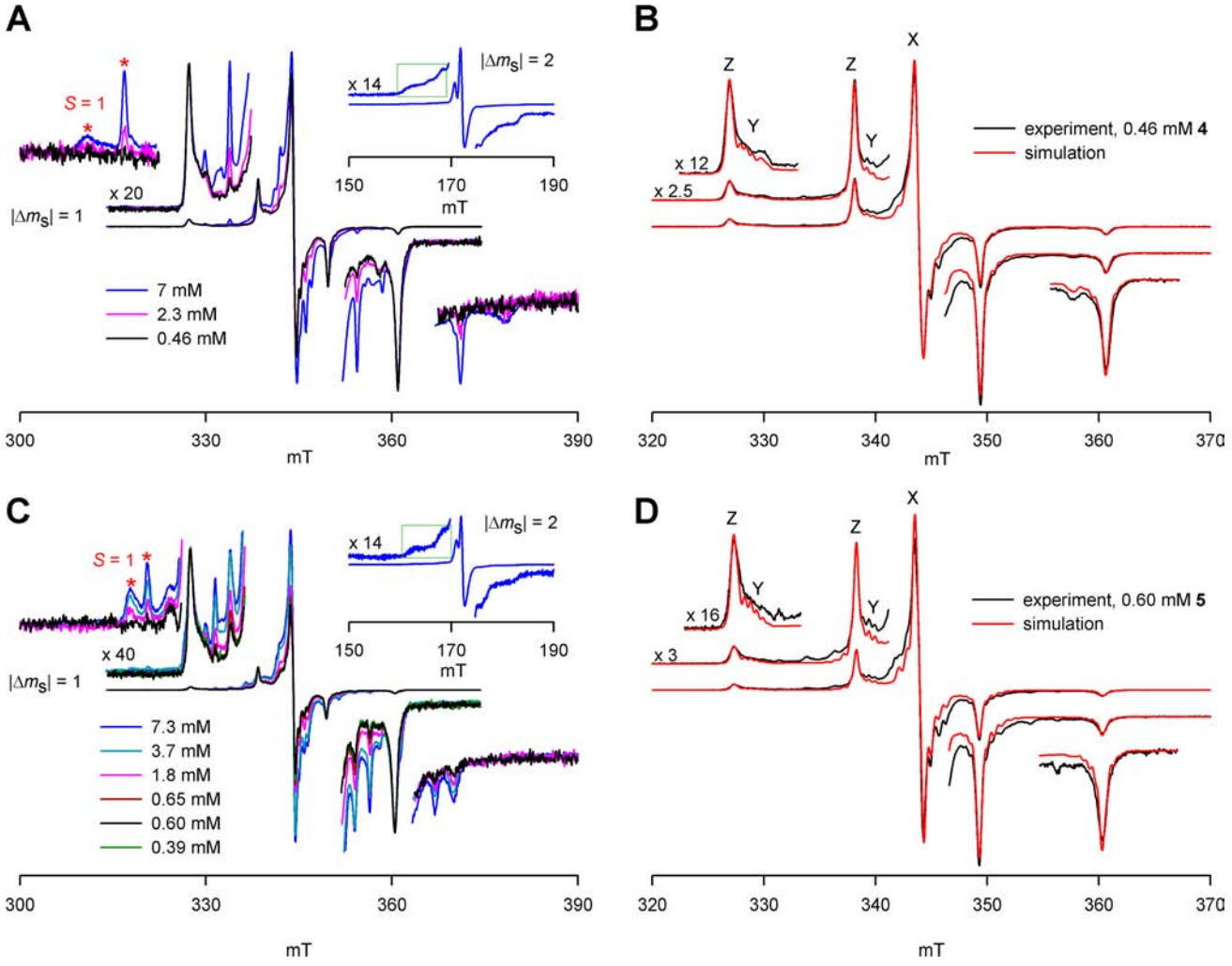

Figure 4. EPR (X-band) spectra of **4** and **5** in 2-MeTHF at 132−133 K. (A and C) Concentration dependent spectra for **4** (A) and **5** (C). The outermost side bands, labeled "$S = 1$", are detected at high sensitivity instrument settings, and their intensities are normalized to the lowest-field $|\Delta m_S| = 1$ band (at 327 mT) for the $S = 2$ ground state of the tetraradical. (B and D) Experimental (black line) and simulated (red line) spectra for 0.46 mM **4** (B) and 0.6 mM **5** (D). Selected EPR spectral parameters for the $S = 2$ ground states of **4** and **5** are summarized in Table 1. Further details regarding simulations of the EPR spectra, including the parameters for byproduct triradicals ($S = 3/2$ states) and monoradical ($S = 1/2$), may be found in Table S3, Supporting Information.

Table 1. Summary of Analyses of EPR Spectra for Aminyl Diradical 2, Tetraradicals 4 and 5, and Dimers $(4)_2$ and $(5)_2$ in 2-MeTHF at 132−133 K

	Conc.[a] (mM)	ν (GHz)	S	$\lvert D/hc\rvert$ (10^{-3} cm^{-1})	$\lvert E/hc\rvert$ (10^{-3} cm^{-1})	$\lvert A_{YY}/hc\rvert$ (10^{-3} cm^{-1})	$\lvert A_{ZZ}/hc\rvert$ (10^{-3} cm^{-1})	g_X	g_Y	g_Z	g[c]
Diradical **2**[b]	0.53	9.4645	1	8.6	1.95		0.99 × 2	2.0030	2.0043	2.0019	2.0031
Tetraradical **4**	0.46	9.6414	2	5.26	1.63	0.50 × 4		2.0023	2.0017	2.0041	2.0027
Tetraradical **5**	0.6	9.6441	2	5.15	1.60	0.50 × 4		2.0020	2.0016	2.0041	2.0026
Dimer $(4)_2$		9.6550	1	31.46	6.40		0.25 × 8[d]	2.0035	2.0037	2.0015	
Dimer $(5)_2$		9.6519	1	24.4	6.3		0.25 × 8[d]	2.0030	2.0042	2.0020	

[a]Concentrations are based on the mass of precursor diamine **13** or tetraamines **10** and **11**, and volume of the solvent. [b]Reference 15. [c]$g = (g_X + g_Y + g_Z)/3$. [d]^{14}N splitting is not resolved in the $S = 1$ states of the dimers.

trahydrofuran (2-MeTHF), the tetraanion is oxidized with iodine. Small portions of iodine are transferred over the vacuum line to a solution of the tetraanion at about −115 °C (158 K), and the reaction mixture is monitored by EPR spectroscopy at about 132−133 K to observe the formation of the tetraradicals **4**−**6**. Custom made quartz tubes that allow for monitoring of the reaction mixture by EPR spectroscopy and flame-sealing are used in preparation of the tetraradicals for the SQUID measurements.

The success in preparation of tetraradicals **4**−**6** and the failure to obtain tetraradicals **15** and **16** from the corresponding tetraamines, using similar reaction conditions, suggest that the carbon and nitrogen atoms with significant spin densities (Figure 2) should be sterically shielded by the 4-*tert*-alkylphenyl pendants.

EPR Spectroscopy. Concentrated purple-blue solutions of tetraradicals **4** and **5** in 2-MeTHF at 133 K show complex EPR

dx.doi.org/10.1021/ja409472f | J. Am. Chem. Soc. 2013, 135, 18205−18215

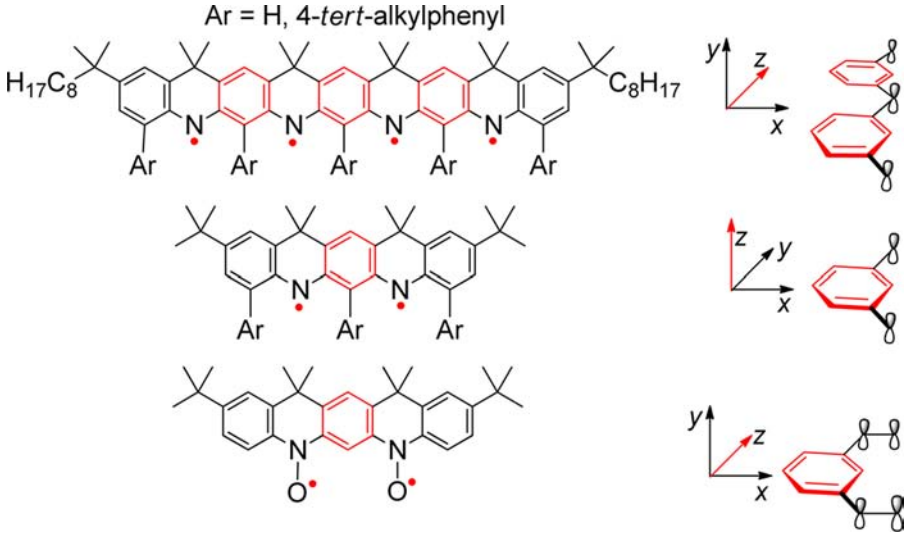

Figure 5. Orientation of the principal axes for **D**-, **A**-, and **g**-tensors in $S = 2$ aminyl tetraradicals, $S = 1$ aminyl diradicals, and $S = 1$ nitroxide diradicals.

spectra in the $|\Delta m_S| = 1$ region (Figure 4 panels A and C for ~7 mM tetraradicals). Notably, upon sequential dilution of the ~7 mM solutions, the outermost side bands labeled "$S = 1$" are progressively decreasing to the baseline level in the dilute solution of <0.7 mM tetraradicals. The EPR spectra of dilute, glassy solutions of **4** and **5** in 2-MeTHF can be simulated and fitted to the $S = 2$ state (Figure 4B,D, and Table 1), indicating that monomeric $S = 2$ tetraradical is the predominant species corresponding to 70−80% of doubly integrated EPR intensity. For each tetraradical, two by-product $S = 3/2$ triradicals and an $S = 1/2$ monoradical are included in the spectral simulation as minor species (Table S3, Supporting Information).[37]

In the $|\Delta m_S| = 2$ region, intense center peaks are observed. In addition, six broad sidebands are detected at 133 K for concentrated samples (inset plots in Figures 4A,C and Figures S66 and S71, Supporting Information). These spectra are more broadened and complicated compared to the $|\Delta m_S| = 2$ spectra with four sidebands for monomeric $S = 2$ hydrocarbon tetraradicals with negligibly small $|E/hc|$.[38,39]

For $S = 2$ tetraradicals **4** and **5**, the zero-field splitting (zfs) parameters $|D/hc| = 5.2–5.3 \times 10^{-3}$ cm^{-1} correspond to the spectral width of $6|D/hc|$, which is nearly two times greater than that of the homologous $S = 1$ diradical **2** (Table 1).[15] In addition, the relative orientations of **D**-, **A**-, and **g**-tensors with respect to the plane of the tetraazanonacene moiety are distinctly different from those in the $S = 1$ diradical **2**, as indicated by the selected principal values listed in Table 1. The Y turning points in **4** and **5**, which include the second outermost peaks, are split into nonets with spacings of $|A_{YY}/hc|/4$, where A_{YY} is the largest principal value of the ^{14}N hyperfine tensor (the **A** tensor) of four nitrogen nuclei. This is in contrast to the splitting of the two outermost peaks (Z turning points) into pentuplets with spacings of $|A_{ZZ}/hc|/2$, where A_{ZZ} is the largest principal value of the ^{14}N hyperfine tensor (the **A** tensor) of two nitrogen nuclei in diradical **2** and in other related planar $S = 1$ aminyl diradicals.[15−17] Because the largest principal value of the ^{14}N hyperfine tensor is expected to coincide with the direction of the nitrogen $2p_\pi$ orbital,[40] the $2p_\pi$ orbital in tetraradicals can be considered to be approximately parallel to the Y-axis, which is the direction of the second largest principal value of the **D** tensor. In comparison, the $2p_\pi$ orbital in diradicals is approximately parallel to the Z-axis, which is the direction of the largest principal value of the **D** tensor. Assuming that the **D** tensor primarily originates in the magnetic dipole−dipole interactions,[41] these relative orientations of **D**- and **A**-tensors in the $S = 2$ aminyl tetraradicals **4** and **5** suggest a "prolate-like" shape of spin density that is elongated in the direction of the Z-axis (Figure 5). This is in contrast to an "oblate-like" shape of spin density that is compressed in the direction of the Z-axis, which is parallel to the $2p_\pi$ orbitals of the azaacene backbone in the $S = 1$ aminyl diradical **2**.

In summary, aminyl tetraradicals **4** and **5** possess a "prolate-like" shape of spin density that is elongated in the direction of the "long" molecular axis of the azaacene backbone, which is in contrast to the homologous aminyl diradicals with an "oblate-like" shape of spin density that is compressed in the direction of $2p_\pi$ orbitals of the azaacene backbone.

The relative orientations of the **D**- and **A**-tensors, and a "prolate-like" shape of spin density for aminyl tetraradicals **4** and **5** are similar to those in planar $S = 1$ nitroxide diradicals (Figure 5), however, the orientations of the principal values of the **g**-tensor are quite different in aminyl and nitroxide radicals. As expected for π-radicals, including aminyl and nitroxide radicals, the smallest principal value of the **g**-tensor is parallel to the $2p_\pi$ orbitals, and thus coinciding with the direction of the largest principal value of the **A**-tensor, such as g_Y in **4** and **5**, and $S = 1$ nitroxide diradical (Figure 5), and g_Z in aminyl diradical **2**. The largest principal value of the **g**-tensor in aminyl diradicals and tetraradicals **1**−**5** is oriented along the "long" molecular axis of the azaacene backbones and orthogonal to the direction of the $2p_\pi$ orbitals (Y-axis in diradicals and Z-axis in tetraradicals). This particular orientation is different from that observed in planar $S = 1$ nitroxide diradicals, for which the largest principal value of the **g**-tensor coincides with the X-axis (Figure 5), a "short" molecular axis orthogonal to the direction of the $2p_\pi$ orbitals.[13,23] In addition, components of the **g**-tensor average to significantly lower isotropic values of $g = (g_X + g_Y + g_Z)/3 \approx 2.003$ (Table 1), compared to $g = 2.0045$ for the diazapentacene-based nitroxide diradical (Figure 5).[23] These isotropic g-values are similar to those observed in planar $S = 1/2$ diarylaminyl and diarylnitroxide radicals.[42] In summary, **g**-tensor analyses differentiate between EPR spectra of aminyl and nitroxide radicals.

Dimers of $S = 2$ Tetraradicals. As indicated by EPR spectroscopy, in the concentrated, purple-blue solutions of the $S = 2$ tetraradicals **4** and **5** in 2-MeTHF at 133 K (Figure 4), the

tetraradicals are likely to exist as dimers $(\mathbf{4})_2$ and $(\mathbf{5})_2$. According to SQUID magnetometry of concentrated, 6−10 mM, **4** and **5** in 2-MeTHF, the intradimer exchange coupling between the $S = 2$ tetraradicals, $J/k \approx -0.1$ K, is antiferromagnetic ($J < 0$) and very weak (Figure 6, and Table 2). Since the value of intradimer $|J/k|$ is

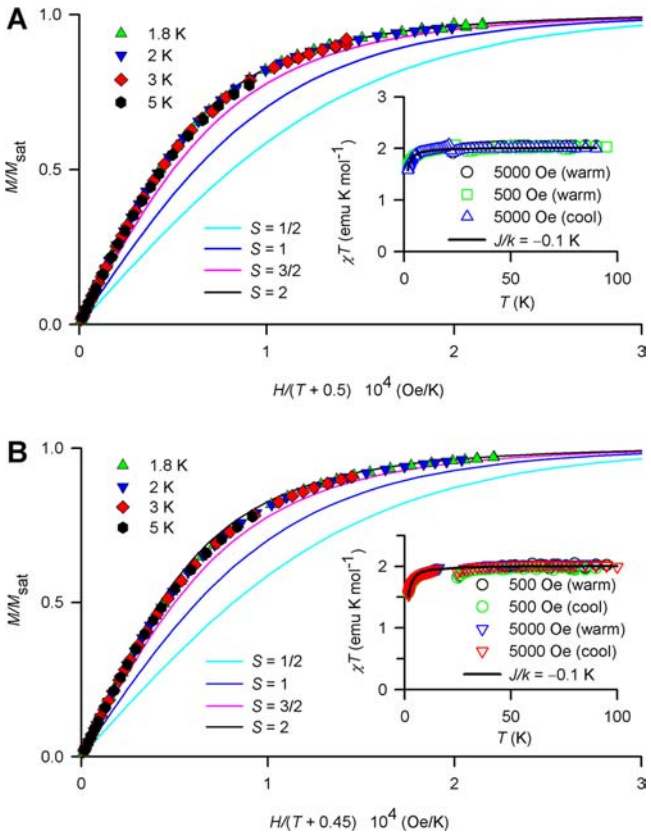

Figure 6. SQUID magnetometry of 6.6 mM **4** (A) and 7.9 mM **5** (B) in 2-MeTHF. Main plots: the magnetization at 1.8, 2, 3, and 5 K is plotted as M/M_{sat} vs $H/(T-\theta)$ with Brillouin functions for $S = 1/2$, 1, 3/2, and 2. Inset plots: the magnetic susceptibility at 500 and 5000 Oe is plotted as χT vs T together with the numerical fit (solid line) to the Heisenberg Hamiltonian for the dimer of $S = 2$ tetraradicals (eq S1, Supporting Information). Fitting parameters for the main and inset plots are summarized in Table 2.

much lower than 133 K, the temperature at which EPR spectra (Figure 4) are obtained, all spin states of the dimer with $S = 0$, 1, 2, 3, and 4 are thermally populated proportionally to their spin multiplicities $2S + 1$. In the EPR spectra of the dimers, each spin state with $S \geq 1$ contributes to the double integrated EPR intensity proportional to its thermal population multiplied by the $S(S + 1)$ factor. One of these spin states gives rise to the outermost side bands that are assigned as "$S = 1$" (Figures 4AC).

Spectral simulation of the outermost bands in dimer $(\mathbf{4})_2$ indicates that the "$S = 1$" bands (Figure 4A) could be assigned to either the $S = 1$ or $S = 2$ state, but not the $S = 3$ or $S = 4$ state. To assign the "$S = 1$" bands, we analyzed the **D**-tensor for the dimer, assuming that $(\mathbf{4})_2$ adopts a π-dimer-like, centrosymmetric structure. The largest components of the **D**-tensors for the $S = 1$, 2, 3, and 4 states of the dimer, labeled as D_1, D_2, D_3, and D_4, as well as for monomeric tetraradical (D_m) and exchange contribution (D_{exch}) may be approximately related by eqs 1a−1d.[43]

$$D_1 = -21/5D_m + 13/5D_{exch} \quad (1a)$$

$$D_2 = -3/7D_m + 5/7D_{exch} \quad (1b)$$

$$D_3 = 1/5D_m + 2/5D_{exch} \quad (1c)$$

$$D_4 = 3/7D_m + 2/7D_{exch} \quad (1d)$$

The components of the **D**-tensors, D_1−D_4, are correlated to the zfs parameters D by a factor of 1.5, as well as to the spectral widths $2(2S - 1)|D|$, thus providing an approximate separation between the outermost bands for each state of the dimer with $S = 1$−4. The spectral simulation suggested that eqs 1a and 1b, i.e., $S = 1$ and $S = 2$ states of $(\mathbf{4})_2$, should be considered. Because the separation between the low-field and high-field "$S = 1$" bands is about $2|D_1| \approx 70$ mT in Figure 4A, which is about twice the spectral width, $6|D_m| \approx 35$ mT, for monomeric $S = 2$ tetraradical **4**, only eq 1a and D_{exch} and D_m with opposite signs yield reasonable values of D_{exch}; that is, typically $|D_{exch}| < |D_m|$. Thus, the "$S = 1$" bands are assigned to the $S = 1$ state of the dimer. For monomeric $S = 2$ tetraradical **4**, D_m is -5.26×10^{-3} cm^{-1}, with the negative sign expected for a prolate-like shape of spin density in **4**, and the spectral simulation of the outermost ("$S = 1$") bands gives $|D_1| = 31.46 \times 10^{-3}$ cm^{-1} for the $S = 1$ state of dimer. From these values, the $D_{exch} \approx 3.6 \times 10^{-3}$ cm^{-1} (and $D_1 > 0$) is estimated from eq 1a.[44] ($D_{exch} > 0$ is anticipated in a π-dimer-like structure of $(\mathbf{4})_2$.[15]) Using eqs 1b−1d, the values of D_2, D_3, and D_4 can then be derived from the D_m and D_{exch}, and used as initial values in the EPR spectral simulation of concentrated solutions of **4** (Table S4 and Figure S3, Supporting Information).

Simulations and double integration of EPR spectra of 1−7 mM tetraradical **4** in 2-MeTHF for the $S = 1$ state of the dimer and $S = 2$ state of the monomer provide an estimated association constant $K_{assoc} \approx 60 \pm 15$ M^{-1} at 132−133 K (Table S5, Supporting Information),[45] which is about five times smaller than that for the dimer of $S = 1$ diradicals **2**.[15]

In the EPR spectra of concentrated solutions of sterically hindered tetraradical **5**, the outermost bands corresponding to the dimer $(\mathbf{5})_2$ are poorly defined and accompanied by additional

Table 2. Summary of Magnetic Data and Numerical Fits for Tetraradicals 4 and 5 in 2-MeTHF

tetraradical	sample number	mass[a] (mg)	concn[b] (mM)	S	$-\theta$ (K)	M_{sat}[c] (μ_B)	χT[d] (emu K mol^{-1})	$\chi T/M_{sat}$	$-J/$(K)
4	1	0.75	6.6	1.9−2.0	0.5	0.71	2.05	2.89	0.1
	2	1.20	10	1.8−1.9	0.5	0.72	1.82	2.53	0.1
	3[e]	1.38	8	2.0	0.9	0.85	2.40	2.82	0.12
5	1	0.97	7.9	1.8	0.5	0.70	2.03	2.90	0.1
	2	1.00	6.7	1.8	0.4	0.72	2.00	2.78	0.08

[a]Mass of tetraamine **10** or **11**. [b]Concentration based on the mass of tetraamine and volume of the solvent. [c]M_{sat} per mol of "monoamine moieties", i.e., aminyl radical site. [d]χT_{max} per mol of tetraamine measured at 5000 Oe. [e]For this sample, residual hexanes may not have been removed as thoroughly as for other samples leading to increased value of the mean-field parameter $-\theta$.

dx.doi.org/10.1021/ja409472f | J. Am. Chem. Soc. 2013, 135, 18205−18215

weak bands. Because of relatively smaller separation of these bands, the spectral simulation gives much smaller $|D_1| \approx 24.4 \times 10^{-3}$ cm^{-1}, compared to that in $(\mathbf{4})_2$.

In summary, concentrated solutions (ca. 1−10 mM) of tetraradical **4** in 2-MeTHF at 133 K are partially associated forming a dimer, in which two $S = 2$ tetraradicals interact with a weak antiferromagnetic exchange coupling (<1 cal mol^{-1}).

SQUID Magnetometry. Magnetic studies of **4** and **5** in 2-MeTHF by SQUID magnetometry unequivocally confirm their quintet ground states, as evidenced by the $S = 2$ paramagnetic behavior in both the magnetization (M) vs magnetic field (H) and the magnetic susceptibility (χ) vs temperature (T) plots (Figure 6 and Table 2).

The M/M_{sat} vs $H/(T - \theta)$ plots for **4** and **5** at 1.8, 3, and 5 K closely follow that of the $S = 2$ Brillouin function. The curvature of the plots, which does not depend on the radical concentration or the amount of sample, indicates that the measured $S \approx 2$ is the ground state. A mean-field parameter, with a typical value, $\theta \approx -0.5$ K, accounts for weak intermolecular antiferromagnetic interactions between the tetraradicals, including intradimer antiferromagnetic exchange coupling, which will be discussed below. Another parameter in the plot, the magnetization at saturation, M_{sat}, measures the spin concentration of the sample, discussed in the next paragraph.

The constant value of χT, as evidenced by the flatness of the χT vs T plots in the $T = 10-100$ K range, indicates that there is no significant change in the thermal population of spin states up to 100 K, the highest temperature allowed by the 2-MeTHF matrix for the measurement. This suggests an approximate lower limit for the triplet-quintet energy gap, $\Delta E_{TQ} > 150$ K (~0.3 kcal mol^{-1}). A correction of the typical values of $\chi T \approx 2$ emu K mol^{-1} with the measured spin concentration, $M_{sat} \approx 0.7\ \mu_B$ (per aminyl radical site), gives $\chi T \approx 2.5-2.9$ emu K mol^{-1} (Table 2), which are close to the value of 3.0 emu K mol^{-1} expected for an $S = 2$ tetraradical. This result provides additional evidence for the $S = 2$ ground state.

The downward curvature of the χT vs T plots in the $T = 10-1.8$ K range may be fit numerically to a Heisenberg Hamiltonian model of dimer of $S = 2$ tetraradicals,[46] with intradimer antiferromagnetic exchange coupling, $J/k \approx -0.1$ K (inset plots in Figure 6, Table 2). In this model, the thermal populations of states with $S = 0$, 1, 2, 3, and 4, as well as their magnetic m_S-levels, are computed to account for paramagnetic saturation effects (eq S1, Supporting Information). The exchange couplings tend to be slightly less negative for the more sterically hindered dimer $(\mathbf{5})_2$, compared to those for $(\mathbf{4})_2$. The small value of $|J/k|$ implies that above $T = 10-20$ K, χT (and other paramagnetic properties) for the dimers will be that of two magnetically independent $S = 2$ tetraradicals, as shown in Figure 6. In the previously reported dimer of $S = 1$ diradicals **2**, the value of $J/k \approx -0.2$ K suggested a stronger intradimer exchange coupling.[15] Studies of conformationally constrained diradicals and tetraradicals indicate that through-space $|J/k|$ of the order of 0.1−1 K are associated with radical−radical distances of about 5−6 Å.[47,48] Similar distances are observed for the closest C···C contacts between the tetraazanonacene moieties in the X-ray structure of tetraamine **11** and the plane-to-plane distance between diazapentacene moieties in the DFT-computed model structure of the dimer of $S = 1$ diradical **2**.[15,49−51]

In summary, SQUID magnetometry establishes unequivocally that tetraradicals **4** and **5** in 2-MeTHF possess quintet ground states with the nearest electronic excited state (triplet) at least ~0.3 kcal mol^{-1} higher in energy ($\Delta E_{TQ} > 0.3$ kcal mol^{-1}). The quintet ground state with this ΔE_{TQ} corresponds to a ferromagnetic exchange coupling within the tetraradical that is more than 3 orders of magnitude stronger than the intradimer antiferromagnetic exchange coupling between the quintet tetraradicals. This weak intradimer exchange coupling ($J/k \approx -0.1$ K ~ 0.2 cal mol^{-1}) is expected for two tetraradicals at the distance of about 6 Å.

Decay Kinetics of Aminyl Tetraradicals. The persistence of **4**−**6** in 2-MeTHF was investigated by EPR spectroscopy. A sample of 0.39 mM tetraradical **5** shows identical EPR spectra before and after annealing at 246 K (−27 °C) for 1 h (Figure S76, Supporting Information). However, the decay of the tetraradical was readily detectable at 295 K, where EPR spectra indicate first order kinetics with a half-life, $\tau_{1/2} \approx 1$ h (Figure 7, and Figure S77, Supporting Information). This half-life is considerably shorter than $\tau_{1/2} \approx 3$ h for $S = 1$ diradical **2** under similar conditions.[15] After several days at room temperature, ^{1}H NMR spectra and mass spectrometry showed that the isolated samples were predominantly tetraamine **11** (Figures S72 and S79, Supporting Information). These results suggest that the decay of **5** to **11** in 2-MeTHF proceeds by a hydrogen abstraction mechanism,[52] which is analogous to those observed for matrix isolated dialkyl aminyl radicals and for diradicals **2** and **3**.[15,16,53]

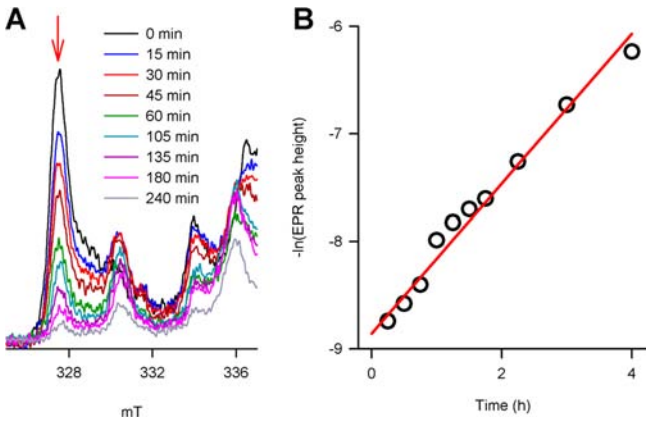

Figure 7. Decay kinetics of 0.39 mM tetraradical **5** in 2-MeTHF at 295 K. (A) Selected EPR spectra at 133 K after annealing at 295 K, with the measured peak height marked with an arrow (~327 mT) and (B) the first-order decay kinetics with a two-parameter fit ($R^2 = 0.981$) that gives rate constant $k = 0.697 \pm 0.075$ h^{-1} (95% confidence level). The intensity of the measured EPR peak height was corrected with a nitroxide radical reference (1.0 mM TEMPONE in 2-MeTHF).

Tetraradicals **4** and **6** are significantly less persistent than **5**, and complex reaction products are formed over time in sealed tubes at room temperature. For **4**, EPR spectra are unchanged, after annealing at 195 K (−78 °C) for 45 min; however, upon the tetraradicals being annealed at 246 K a significant decay of the EPR signal intensity is observed, for example, ~10% decrease after 15 min (Figure S69, Supporting Information). Tetraradical **6**, for which one of the positions in the tetraazanonacene moiety with large spin density is sterically unprotected (Figure 2) is less persistent than **4**. EPR spectra of **6** in 2-MeTHF show a significant decay at −78 °C with $\tau_{1/2} \approx 15$ min and the plot of the decay of EPR intensity can be numerically fitted to first order kinetics with modest quality ($R^2 = 0.96$, $k \approx 0.04 \pm 0.01$ min^{-1} at the 95% confidence level), suggesting a more complex kinetic behavior. After several days at room temperature, the crude reaction mixture shows a complicated ^{1}H NMR spectrum. The

Table 3. Summary of Triplet-Quintet Energy Gaps (ΔE_{TQ}) for 4a and 17 by the BS-DFT at the UB3LYP/6-31G(d)+ZPVE Level[a]

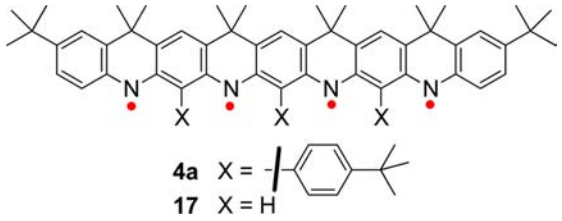

	state	N-centered spin densities	$\langle S^2\rangle_{Expected}$	$\langle S^2\rangle_{Calculated}$	ΔE_{UHF} (kcal mol^{-1})	ΔE_{TQ} (kcal mol^{-1})
4a	quintet	$\alpha\alpha\alpha\alpha\alpha$	6.00	6.17	0.00	0.00
	BS triplet	$\beta\alpha\alpha\alpha$	3.00	3.13	3.54	4.85
17	quintet	$\alpha\alpha\alpha\alpha\alpha$	6.00	6.17	0.00	0.00
	BS triplet	$\beta\alpha\alpha\alpha$	3.00	3.13	3.62	4.97

[a]Further computational details on **4a** and **17** are provided in Tables S8 and S9, and Figure S4 in the Supporting Information.

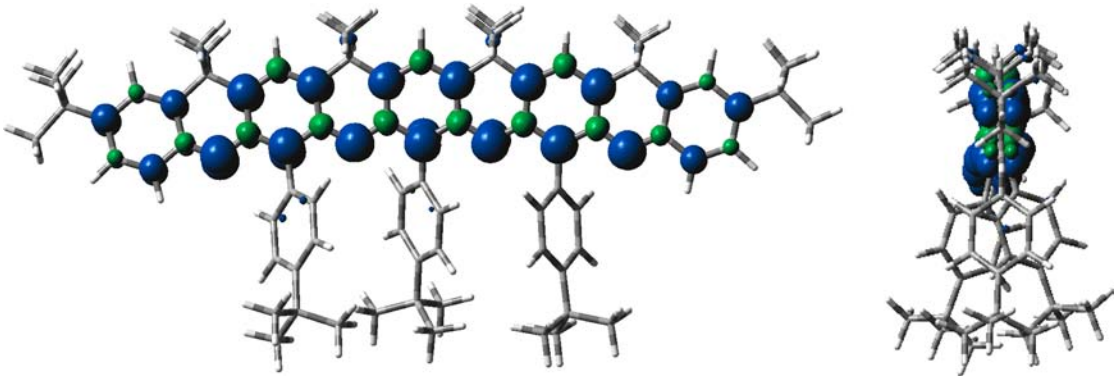

Figure 8. Spin density map for the quintet ground state of tetraradical **4a** at the UB3LYP/6-31G(d) level of theory. Positive (blue) and negative (green) spin densities are shown at the isodensity level of 0.006 electron/Bohr.[3]

MALDI MS peaks are comparable to an m/z of **12** and a dimer of **6** (or **12**) (Figures S94–S96, Supporting Information).

For **5**, the most persistent tetraradical, we investigated its reaction with oxygen (O_2). The EPR spectrum of 2.8 mM **5** in 2-MeTHF is unchanged after the solution is saturated with dry O_2 at 165 K (−108 °C) for 25 min (and then degassed); however, a similar experiment at 195 K results in a sharp decrease of the EPR signal intensity and, in particular, the complete disappearance of the quintet resonances for **5** (Figure S87, Supporting Information). This behavior is analogous to that observed upon exposure of **2** in 2-MeTHF to O_2.[15]

DFT Computation of Quintet–Triplet Energy Gaps. The simplified structures of aminyl tetraradical **4**, that is, **4a** and **17** (Table 3), were studied at the UB3LYP/6-31G(d)+ZPVE level of theory. Full geometry optimizations for the high-spin ($S = 2$) states, starting from either planar or buckled conformations for the fused ring moieties, result in energy minima with planar conformations. The low-spin ($S = 1$ and $S = 0$) states were studied using broken-symmetry wave functions and were also optimized to planar geometries for the fused ring moieties.

Similarly to the linear tetramers of Cu(II) ions with spin-1/2,[54] the triplet state of tetraradicals **4**, **4a**, and **17** is expected to be the lowest energy low-spin excited state (and the first excited state), just above the quintet ground state. Assuming that the spin contamination of the lowest energy excited triplet state only originates from the quintet ground state components, the triplet–quintet energy gap (ΔE_{TQ}) may be estimated using the energy difference between ground state quintet and lowest energy broken-symmetry triplet (ΔE_{UHF}) and the correction for spin contamination (eq 2).[2b,55]

$$\Delta E_{TQ} = \Delta E_{UHF}[(\langle S_Q^2\rangle - 2.00)/(\langle S_Q^2\rangle - \langle S_{BS\text{-}T}^2\rangle)] \quad (2)$$

The correction for spin contamination is based on the calculated mean values of the S^2 operator for the ground state quintet ($\langle S_Q^2\rangle$) and broken symmetry triplet ($\langle S_{BS\text{-}T}^2\rangle$).

Both **4a** and **17** possess similar $\Delta E_{TQ} \approx 5$ kcal mol^{-1} as expected because the spin density is primarily within the fused ring moiety (Figure 8). However, ΔE_{TQ} for **4** is probably somewhat smaller because DFT, including the broken symmetry approach, typically overestimates the stability of the high spin ground state.[21,56–58]

Using the UB3LYP/6-31G(d)-optimized geometries of the high-spin ($S = 2$) states of **4a** and **17**, the EPR **D**-tensor and ^{14}N **A**-tensors are computed at the B3LYP/EPR-II level using ORCA.[59,60] Computations of the **D**-tensor employed the spin–spin approximation, neglecting spin–orbit contributions, which provides reasonable agreement between theory and experiment for organic diradicals with spin densities centered on first row elements,[61,62] including *N*-centered diradicals.[16,41] Specifically, for planar aminyl and nitroxide triplet diradicals, e.g., **3** (Figure 1), the B3LYP/EPR-II-computed EPR spectra provide the correct orientation of the **D**-tensor (and thus, the correct sign), as indicated by the ^{14}N pentuplet splitting of the outermost lines (Z-lines) in aminyls and the splitting of the second outermost lines (Y-lines) in nitroxides. However, the values of the zero-field splitting parameter D are usually overestimated, especially in aminyls.

For both **4a** and **17**, the computed zero-field splitting parameters $D \approx 11 \times 10^{-3}$ cm^{-1} and $E \approx 3 \times 10^{-3}$ cm^{-1} are similar, as expected for similar spin density distribution in both

tetraradicals (Figure 8 and Figure S4, Supporting Information). These computed values overestimate the experimental D and E in **4** by a factor of 2 (Table 1), similarly to that in aminyl diradical **3**.[16] Morever, the largest (D_{ZZ}) and second largest (D_{YY}) principal values of the **D** tensor have the opposite orientation for computed **4a** and **17** vs the orientation experimentally found in **4**. For example, the largest value (D_{ZZ}) is approximately parallel (in **4a** and **17** by computation) and orthogonal (in **4** by EPR spectroscopy) to the direction of the $2p_{\pi}$-orbitals on the nitrogens. Consequently, the computed EPR spectra for **4a** and **17** show nonet splitting due to the largest component of the ^{14}N ***A***-tensor at the Z-lines of the spectrum (including the most outer lines), in contrast to the experimentally observed nonet splittings of the Y-lines (including the second most outer lines) in **4**.

■ ASSOCIATED CONTENT

Supporting Information

General procedures and materials, additional experimental details, and X-ray crystallographic files (tetraamine **11**) in CIF format. This material is available free of charge via the Internet at http://pubs.acs.org.

■ AUTHOR INFORMATION

Corresponding Author

arajca1@unl.edu

Notes

The authors declare no competing financial interest.

[§]P.J.B.: On leave from Wrocław University of Technology.

■ ACKNOWLEDGMENTS

This research was supported by the National Science Foundation (CHE-0718117 and CHE-1012578), including the purchase of the Electron Paramagnetic Resonance (EPR) spectrometer (DMR-0216788) used in this work. ChemMatCARS Sector 15 is principally supported by the National Science Foundation/Department of Energy under Grant No. NSF/CHE-0822838. Use of the Advanced Photon Source was supported by the U.S. Department of Energy, Office of Science, Office of Basic Energy Sciences, under Contract No. DE-AC02-06CH11357. We thank Dr. Kouichi Shiraishi for the attempts to generate aminyl radicals from the methyl-substituted tetraamine **14**.

■ REFERENCES

(1) (a) Rajca, A. *Chem. Rev.* **1994**, *94*, 871−893. (b) Rajca, A. *Chem.−Eur. J.* **2002**, *8*, 4834−4841. (c) Itoh, K., Kinoshita, M., Eds. *Molecular Magnetism*; Gordon and Breach: Kodansha: New York, 2000; pp 1−337. (d) Tretyakov, E. V.; Ovcharenko, V. I. *Russ. Chem. Rev.* **2009**, *78*, 971−1012. (e) Lahti, P. M. *Adv. Phys. Org. Chem.* **2011**, *45*, 93−169.

(2) (a) Fukuzaki, E.; Nishide, H. *J. Am. Chem. Soc.* **2006**, *128*, 996−1001. (b) Trinquier, G.; Suaud, N.; Malrieu, J.-P. *Chem.−Eur. J.* **2010**, *16*, 8762−8772. (c) Perrotta, R. R.; Winter, A. H.; Coldren, W. H.; Falvey, D. E. *J. Am. Chem. Soc.* **2011**, *133*, 15553−15558. (d) Adam, W.; Baumgarten, M.; Maas, W. *J. Am. Chem. Soc.* **2000**, *122*, 6735−6738.

(3) (a) Wenthold, P. G.; Hu, J.; Squires, R. R.; Lineberger, W. C. *J. Am. Chem. Soc.* **1996**, *118*, 475−476. (b) West, A. P., Jr.; Silverman, S. K.; Dougherty, D. A. *J. Am. Chem. Soc.* **1996**, *118*, 1452−1463. (c) Itoh, T.; Matsuda, K.; Iwamura, H.; Hori, K. *J. Am. Chem. Soc.* **2000**, *122*, 2567−2576. (d) Shultz, D. A.; Fico, R. M., Jr.; Bodnar, S. H.; Kumar, K.; Vostrikova, K. E.; Kampf, J. W.; Boyle, P. D. *J. Am. Chem. Soc.* **2003**, *125*, 11761−11771. (e) Shultz, D. A.; Fico, R. M., Jr.; Lee, H.; Kampf, J. W.; Kirschbaum, K.; Pinkerton, A. A.; Boyle, P. D. *J. Am. Chem. Soc.* **2003**, *125*, 15426−15432. (f) Rajca, A.; Shiraishi, K.; Vale, M.; Han, H.; Rajca, S. *J. Am. Chem. Soc.* **2005**, *127*, 9014−9020. (g) Matsumoto, K.; Inokuchi, D.; Hirao, Y.; Kurata, H.; Sato, K.; Takui, T.; Kubo, T. *Org. Lett.* **2010**, *12*, 836−839. (h) Suzuki, S.; Nagata, A.; Kuratsu, M.; Kozaki, M.; Tanaka, R.; Shiomi, D.; Sugisaki, K.; Toyota, K.; Sato, K.; Takui, T.; Okada, K. *Angew. Chem., Int. Ed.* **2012**, *51*, 3193−3197.

(4) Pauling, L. *J. Am. Chem. Soc.* **1931**, *53*, 1367−1400.

(5) Pauli, W. *Z. Phys.* **1925**, *31*, 765−783.

(6) (a) Herrmann, C.; Solomon, G. C.; Ratner, M. A. *J. Am. Chem. Soc.* **2010**, *132*, 3682−3684. (b) Jahn, B. O.; Ottosson, H.; Galperin, M.; Fransson, J. *ACS Nano* **2013**, *7*, 1064−1071.

(7) Clore, G. M.; Iwahara, J. *Chem. Rev.* **2009**, *109*, 4108−4139.

(8) Davis, R. M.; Sowers, A. L.; DeGraff, W.; Bernardo, M.; Thetford, A.; Krishna, M. C.; Mitchell, J. B. *Free Radic. Biol. Med.* **2011**, *51*, 780−790.

(9) (a) Rajca, A.; Wang, Y.; Boska, M.; Paletta, J. T.; Olankitwanit, A.; Swanson, M. A.; Mitchell, D. G.; Eaton, S. S.; Eaton, G. R.; Rajca, S. *J. Am. Chem. Soc.* **2012**, *134*, 15724−15727. (b) Spagnol, G.; Shiraishi, K.; Rajca, S.; Rajca, A. *Chem. Commun.* **2005**, 5047−5049.

(10) (a) Rajca, A.; Wongsriratanakul, J.; Rajca, S. *Science* **2001**, *294*, 1503−1505. (b) Rajca, A.; Rajca, S.; Wongsriratanakul, J. *J. Am. Chem. Soc.* **1999**, *121*, 6308−6309.

(11) (a) Rajca, S.; Rajca, A.; Wongsriratanakul, J.; Butler, P.; Choi, S. *J. Am. Chem. Soc.* **2004**, *126*, 6972−6986. (b) Rajca, A.; Wongsriratanakul, J.; Rajca, S. *J. Am. Chem. Soc.* **2004**, *126*, 6608−6626. (c) Rajca, A.; Wongsriratanakul, J.; Rajca, S.; Cerny, R. L. *Chem.−Eur. J.* **2004**, *10*, 3144−3157. (d) Rajca, A.; Lu, K.; Rajca, S. *J. Am. Chem. Soc.* **1997**, *119*, 10335−10345. (e) Rajca, A.; Rajca, S.; Padmakumar, R. *Angew. Chem.—Int. Ed. Engl.* **1994**, *33*, 2091−2093.

(12) (a) Ratera, I.; Veciana, J. *Chem. Soc. Rev.* **2012**, *41*, 303−349. (b) Rajca, A. *Adv. Phys. Org. Chem.* **2005**, *40*, 153−199.

(13) (a) Rajca, A.; Takahashi, M.; Pink, M.; Spagnol, G.; Rajca, S. *J. Am. Chem. Soc.* **2007**, *129*, 10159−10170. (b) Rassat, A.; Sieveking, U. *Angew. Chem., Int. Ed. Engl.* **1972**, *11*, 303−304.

(14) Suzuki, S.; Furui, T.; Kuratsu, M.; Kozaki, M.; Shiomi, D.; Sato, K.; Takui, T.; Okada, K. *J. Am. Chem. Soc.* **2010**, *132*, 15908−15910.

(15) Boratyński, P. J.; Pink, M.; Rajca, S.; Rajca, A. *Angew. Chem., Int. Ed.* **2010**, *49*, 5459−5462.

(16) Rajca, A.; Olankitwanit, A.; Rajca, S. *J. Am. Chem. Soc.* **2011**, *133*, 4750−4753.

(17) Rajca, A.; Shiraishi, K.; Pink, M.; Rajca, S. *J. Am. Chem. Soc.* **2007**, *129*, 7232−7233.

(18) (a) Neugebauer, F. A.; Fischer, H.; Bamberger, S.; Smith, H. O. *Chem. Ber.* **1972**, *105*, 2694−2713. (b) Ballester, N.; Castaner, J.; Olivella, S. *Tetrahedron Lett.* **1974**, *15*, 615−616.

(19) (a) Chatgilialoglu, C.; Ferreri, C.; Terzidis, M. A. *Chem. Soc. Rev.* **2011**, *40*, 1368−1382. (b) Büttner, T.; Geier, J.; Frison, G.; Harmer, J.; Calle, C.; Schweiger, A.; Schönberg, H.; Grützmacher, H. *Science* **2005**, *307*, 235−238. (c) Haider, K.; Soundararajan, N.; Shaffer, M.; Platz, M. S. *Tetrahedron Lett.* **1989**, *30*, 1225−1228.

(20) Fang, S.; Lee, M.-S.; Hrovat, D. A.; Borden, W. A. *J. Am. Chem. Soc.* **1995**, *117*, 6727−6731.

(21) Barone, V.; Boilleau, C.; Cacelli, I.; Ferretti, A.; Monti, S.; Prampolini, G. *J. Chem. Theory Comput.* **2013**, *9*, 300−307.

(22) Barone, V.; Cacelli, I.; Ferretti, A.; Monti, S.; Prampolini, G. *Phys. Chem. Chem. Phys.* **2011**, *13*, 4709−4714.

(23) (a) Rajca, A.; Shiraishi, K.; Rajca, S. *Chem. Commun.* **2009**, 4372−4374. (b) Rajca, A.; Shiraishi, K.; Boratynski, P. J.; Pink, M.; Miyasaka, M.; Rajca, S. *J. Org. Chem.* **2011**, *76*, 8447−8457.

(24) (a) For triarylmethyl diradical, a derivative of pentacene, ΔE_{ST} = 6.4 kcal mol^{-1} is computed using BS-DFT (Table S7, Supporting Information). (b) Rajca, A.; Utamapanya, S. *J. Org. Chem.* **1992**, *57*, 1760−1767.

(25) Bushby, R. J.; Taylor, N.; Williams, R. A. *J. Mater. Chem.* **2007**, *17*, 955−964.

(26) Rajca, A.; Boratynski, P. J.; Olankitwanit, A.; Shiraishi, K.; Pink, M.; Rajca, S. *J. Org. Chem.* **2012**, *77*, 2107−2120.

(27) Shiraishi, K.; Rajca, A.; Pink, M.; Rajca, S. *J. Am. Chem. Soc.* **2005**, *127*, 9312−9313.

(28) Pan, J.; Su, M.; Buchwald, S. L. *Angew. Chem., Int. Ed.* **2011**, *50*, 8647−8651.

(29) Connelly, N. G.; Geiger, W. E. *Chem. Rev.* **1996**, *96*, 877−910.
(30) Mercury 2.3, http://www.ccdc.cam.ac.uk/mercury/: Macrae, C. F.; Bruno, I. J.; Chisholm, J. A.; Edgington, P. R.; McCabe, P.; Pidcock, E.; Rodriguez-Monge, L.; Taylor, R.; van de Streek J.; Wood, P. A. *J. Appl. Crystallogr.* **2008**, *41*, 466−470.
(31) Keller, E. *Schakal 99, a computer program for the graphic representation of molecular and crystallographic models*; Universitaet Freiburg: Germany, 1999.
(32) (32a) Frisch, M. J.; Trucks, G. W.; Schlegel, H. B.; Scuseria, G. E.; Robb, M. A.; Cheeseman, J. R.; Montgomery, J. A., Jr.; Vreven, T.; Kudin, K. N.; Burant, J. C.; Millam, J. M.; Iyengar, S. S.; Tomasi, J.; Barone, V.; Mennucci, B.; Cossi, M.; Scalmani, G.; Rega, N.; Petersson, G. A.; Nakatsuji, H.; Hada, M.; Ehara, M.; Toyota, K.; Fukuda, R.; Hasegawa, J.; Ishida, M.; Nakajima, T.; Honda, Y.; Kitao, O.; Nakai, H.; Klene, M.; Li, X.; Knox, J. E.; Hratchian, H. P.; Cross, J. B.; Bakken, V.; Adamo, C.; Jaramillo, J.; Gomperts, R.; Stratmann, R. E.; Yazyev, O.; Austin, A. J.; Cammi, R.; Pomelli, C.; Ochterski, J. W.; Ayala, P. Y.; Morokuma, K.; Voth, G. A.; Salvador, P.; Dannenberg, J. J.; Zakrzewski, V. G.; Dapprich, S.; Daniels, A. D.; Strain, M. C.; Farkas, O.; Malick, D. K.; Rabuck, A. D.; Raghavachari, K.; Foresman, J. B.; Ortiz, J. V.; Cui, Q.; Baboul, A. G.; Clifford, S.; Cioslowski, J.; Stefanov, B. B.; Liu, G.; Liashenko, A.; Piskorz, P.; Komaromi, I.; Martin, R. L.; Fox, D. J.; Keith, T.; Al-Laham, M. A.; Peng, C. Y.; Nanayakkara, A.; Challacombe, M.; Gill, P. M. W.; Johnson, B.; Chen, W.; Wong, M. W.; Gonzalez, C.; Pople, J. A. *Gaussian 03*, revision E.01; Gaussian: Wallingford, CT, 2004. (32b) Frisch, M. J.; Trucks, G. W.; Schlegel, H. B.; Scuseria, G. E.; Robb, M. A.; Cheeseman, J. R.; Scalmani, G.; Barone, V.; Mennucci, B.; Petersson, G. A.; Nakatsuji, H.; Caricato, M.; Li, X.; Hratchian, H. P.; Izmaylov, A. F.; Bloino, J.; Zheng, G.; Sonnenberg, J. L.; Hada, M.; Ehara, M.; Toyota, K.; Fukuda, R.; Hasegawa, J.; Ishida, M.; Nakajima, T.; Honda, Y.; Kitao, O.; Nakai, H.; Vreven, T.; Montgomery, J. A., Jr.; Peralta, J. E.; Ogliaro, F.; Bearpark, M.; Heyd, J. J.; Brothers, E.; Kudin, K. N.; Staroverov, V. N.; Kobayashi, R.; Normand, J.; Raghavachari, K.; Rendell, A.; Burant, J. C.; Iyengar, S. S.; Tomasi, J.; Cossi, M.; Rega, N.; Millam, J. M.; Klene, M.; Knox, J. E.; Cross, J. B.; Bakken, V.; Adamo, C.; Jaramillo, J.; Gomperts, R.; Stratmann, R. E.; Yazyev, O.; Austin, A. J.; Cammi, R.; Pomelli, C.; Ochterski, J. W.; Martin, R. L.; Morokuma, K.; Zakrzewski, V. G.; Voth, G. A.; Salvador, P.; Dannenberg, J. J.; Dapprich, S.; Daniels, A. D.; Farkas, O.; Foresman, J. B.; Ortiz, J. V.; Cioslowski, J.; Fox, D. J. *Gaussian 09*; revision A.01, Gaussian: Wallingford, CT, 2009.
(33) Jain, R.; Bally, T.; Rablen, P. R. *J. Org. Chem.* **2009**, *74*, 4017−4023.
(34) Saielli, G.; Nicolaou, K. C.; Ortiz, A.; Zhang, H.; Bagno, A. *J. Am. Chem. Soc.* **2011**, *133*, 6072−6077.
(35) Barone, G.; Gomez-Paloma, L.; Duca, D.; Silvestri, A.; Riccio, R.; Bifulco, G. *Chem.−Eur. J.* **2002**, *8*, 3233−3239.
(36) Lodewyk, M. W.; Siebert, M. R.; Tantillo, D. J. *Chem. Rev.* **2012**, *112*, 1839−1862.
(37) (a) In the simulated EPR spectrum of **4** (Figure 4B), by-product $S = 3/2$ triradicals with $|D/hc| \approx 3 \times 10^{-3}$ cm^{-1} and $|D/hc| \approx 6.7 \times 10^{-3}$ cm^{-1} contribute 14% and 6% double integrated intensity, respectively; for **5** (Figure 4D), the corresponding contributions are 23% and 1% (Table S3, Supporting Information). (b) A small contribution from all EPR-active states of the dimer of $S = 2$ tetraradicals may improve the fit but it is not included in Figure 4 panels B and D.
(38) Rajca, A.; Utamapanya, S. *J. Am. Chem. Soc.* **1993**, *115*, 2396−2401.
(39) Rajca, A.; Rajca, S.; Desai, S. R. *J. Am. Chem. Soc.* **1995**, *117*, 806−816.
(40) Morton, J. R. *Chem. Rev.* **1964**, *64*, 453−471.
(41) The spin−orbit coupling contribution to the **D**-tensor may be neglected in the *N*-centered π-diradicals: Havlas, Z.; Kývala, M.; Michl, J. *Mol. Phys.* **2005**, *103*, 407−411.
(42) (a) Neugebauer, F. A.; Bamberger, S. *Chem. Ber.* **1974**, *107*, 2362−2382. (b) Aurich, H. G.; Hahn, K.; Stork, K.; Weiss, W. *Tetrahedron* **1977**, *33*, 969−975.
(43) Bencini, A.; Gatteschi, D. *EPR of Exchange Coupled Systems*; Springer: Berlin, 1990; pp 48−85.
(44) $D_{exch} \approx 7.8 \times 10^{-3}$ cm^{-1} was estimated for the π-dimer-like structure of $S = 1$ diradical **2**.
(45) $K_{assoc} \approx 90$ M^{-1} for $(\mathbf{4})_2$ at 133 K is obtained from spectral simulation of entire $\Delta m_S = 1$ region of experimental EPR spectrum for 7 mM **4** (Figure S3, Supporting Information).
(46) Belorizky, E.; Fries, P. H. *J. Chim. Phys.* **1993**, *90*, 1077−1100.
(47) (a) Rajca, A.; Mukherjee, S.; Pink, M.; Rajca, S. *J. Am. Chem. Soc.* **2006**, *128*, 13497−13507. (b) Rajca, A.; Mukherjee, S.; Pink, M.; Rajca, S.; Das, K. *Tetrahedron* **2007**, *63*, 10731−10742.
(48) Olankitwanit, A.; Kathirvelu, V.; Rajca, S.; Eaton, G. R.; Eaton, S. S.; Rajca, A. *Chem. Commun.* **2011**, *47*, 6443−6445.
(49) (a) The closest C···C distances between the adjacent tetraazanonacene moieties in the X-ray structure of tetraamine **11** are about 6 Å. (b) Plane-to-plane distance between diazapentacene moieties in the $S = 2$ state of the UB3LUP/6-31G(d)-computed dimer for a simplified diradical **2** is about 5.7 Å (ref 15).
(50) (a) In the dimers $(\mathbf{4})_2$ and $(\mathbf{2})_2$, parallel exchange coupling pathways are expected to offset the effect of relatively low "atomic" spin densities on the intradimer exchange coupling constant *J*. (b) Rajca, A.; Rajca, S.; Wongsriratanakul, J. *Chem. Commun.* **2000**, 1021−1022.
(51) McConnell, H. *J. Chem. Phys.* **1963**, *39*, 1910.
(52) Blanksby, S. J.; Ellison, G. B. *Acc. Chem. Res.* **2003**, *36*, 255−263.
(53) Roberts, J. R.; Ingold, K. U. *J. Am. Chem. Soc.* **1973**, *95*, 3228−3235.
(54) Halvorson, K. E.; Grigereit, T.; Willett, R. D. *Inorg. Chem.* **1987**, *26*, 1716−1720.
(55) Noodleman, L. *J. Chem. Phys.* **1981**, *74*, 5737−5744.
(56) Wang, T.; Krylov, A. I. *J. Chem. Phys.* **2005**, *123*, 104304−1−6.
(57) Wenthold, P. G.; Kim, J. B.; Lineberger, W. C. *J. Am. Chem. Soc.* **1997**, *119*, 1354−1359.
(58) Barone, V.; Cacelli, I.; Cimino, P.; Ferretti, A.; Monti, S.; Prampolini, G. *J. Phys. Chem. A* **2009**, *113*, 15150−15155.
(59) Neese, F. *ORCA—An Ab Initio, Density Functional and Semiempirical Program Package*, version 2.6; University of Bonn: Germany, 2008.
(60) Allouche, A.-R. *J. Comput. Chem.* **2011**, *32*, 174−182.
(61) Sinnecker, S.; Neese, F. *J. Phys. Chem. A* **2006**, *110*, 12267−12275.
(62) Grote, D.; Finke, C.; Kossmann, S.; Neese, F.; Sander, W. *Chem.—Eur. J.* **2010**, *16*, 4496−4506.